Development of 6-inch h-BN thick wafers

Z. Alemoush ; M. Almohammad ; J. Li ; J. Y. Lin ; H. X. Jiang ✉

Check for updates

View Online   Export Citation

Articles You May Be Interested In

Evaluation of lattice curvature and crystalline homogeneity for 2-inch GaN homo-epitaxial layer

AIP Advances (July 2018)

Analysis of reaction between c+a and -c+a dislocations in GaN layer grown on 4-inch Si(111) substrate with AlGaN/AlN strained layer superlattice by transmission electron microscopy

AIP Advances (April 2016)

Wafer-level MOCVD growth of AlGaN/GaN-on-Si HEMT structures with ultra-high room temperature 2DEG mobility

AIP Advances (November 2016)

Development of 6-inch h-BN thick wafers

View Online   Export Citation   CrossMark

Z. Alemoush, [ID] M. Almohammad, [ID] J. Li, [ID] J. Y. Lin, [ID] and H. X. Jiang[a] [ID]

AFFILIATIONS

Department of Electrical and Computer Engineering, Texas Tech University, Lubbock, Texas 79409, USA

[a]Author to whom correspondence should be addressed: hx.jiang@ttu.edu

ABSTRACT

We report the first successful synthesis of 40 μm thick h-BN wafers with a diameter of 6 in. using hydride vapor phase epitaxy. This accomplishment was made possible by employing BCl_3 as the B precursor to eliminate carbon impurities, utilizing inert N_2 as the carrier and separation gas to isolate BCl_3 and NH_3 gas sources, and implementing low-pressure growth to prevent parasitic reactions in the gas phase. These strategies enabled the growth of h-BN wafers 6 in. in diameter with improved uniformity in thickness and crystallinity. Analysis through x-ray diffraction, selected area electron diffraction, and transmission electron microscopy revealed that the wafer deposited at the lowest pressure of 20 Torr exhibited highest crystalline quality with measured c-lattice constant $c = 6.66$ Å and an a-lattice constant $a = 2.48$ Å, in good agreement with the expected lattice parameters of phase-pure h-BN. Time-resolved photoluminescence emission spectroscopy unveiled a dominant emission line near 3.41 eV, with a recombination lifetime of 2.7 ns at room temperature. These spectroscopic characteristics, when considered alongside a previous theoretical study, suggest that nitrogen vacancies (V_N) constitute the primary defects in these large-diameter h-BN wafers. The achievement of 6 in. diameter wafers with substantial thickness represents a significant advancement in h-BN development, paving the way for the industrial adoption of h-BN technologies, with implications for quantum information and technology, single photon emitters, neutron detectors, power electronics, and deep UV photonics.

The scientific community has unequivocally established that the performance metrics of semiconductor electronic devices scale non-linearly with the material's energy bandgap.[1] This understanding has propelled ultrawide bandgap (UWBG) semiconductors to the forefront as the next generation of semiconductor materials, offering significant advantages across electronic, optoelectronic, energy, and defense technologies. Among the UWBG materials, hexagonal boron nitride (h-BN) stands out for its ultrawide bandgap of ~6.1 eV,[2–6] a high breakdown field of ~12 MV/cm,[7,8] and excellent in-plane thermal conductivity of ~550 W/m K.[9] These outstanding properties have the potential to further expand the established applications of III-nitrides in various fields, including visible and UV photonics, electronics, full spectrum solar energy conversion, and microLED displays.[10–26] In its two-dimensional (2D) form, h-BN has garnered considerable research interest, particularly for its hyperbolic dispersion in the infrared (IR) spectral region, strong optical nonlinearities, potential as a single photon emitter in the visible and UV wavelengths, and solid-state qubit for quantum information and technology.[27–29]

An area of significant promise for hexagonal boron nitride (h-BN) is its application in thermal neutron detection. This potential arises from the presence of boron-10 (^{10}B) isotope in h-BN, which is one of a few that exhibits a favorable nuclear interaction cross section for thermal neutrons, measuring 3840 b.[30,31] Consequently, ^{10}B-enriched (natural) h-BN with thicknesses exceeding 47.3 μm (237 μm) is an outstanding material for the construction of high efficiency direct-conversion thermal neutron detectors.[32–36] Over the past decade, substantial advancements have been made in material growth and understanding of fundamental properties of h-BN. However, a major challenge persists in the fabrication of large-diameter thick wafers using growth techniques that are able to produce materials with a comparable crystalline quality of millimeter-sized crystals produced by high pressure high temperature (HPHT) and metal flux solution methods.[2,7,8,37–40] The wafer scaling challenges stem from the poor surface migration of boron atoms, attributed to the strong B–N bond, and the severe parasitic reactions between B and N precursors in the gas phase. The byproducts of these reactions lead to a rough surface and a high density of crystalline defects.[32,41–46]

While a few layers or a few micrometer-thick h-BN wafers grown on sapphire substrates with diameters of up to 6 in. have been achieved using metal organic chemical vapor deposition (MOCVD),[32–34,42] the use of metal organic sources in MOCVD growth introduces carbon impurities that can impact the overall

03 June 2025 19:43:07

quality and device performance. More importantly, the growth rate of MOCVD is typically limited to a few micrometers per hour, posing challenges in fabricating thick h-BN wafers.[32,40–46] We previously reported growth by hydride vapor phase epitaxy (HVPE) of 4 in. diameter h-BN quasi-bulk crystals with improved crystalline quality.[35,36,47] HVPE growth offers key advantages, including carbon-free growth at high growth rates, as demonstrated in GaN and AlN quasi-bulk wafers.[48,49] Until now, the growth of 6 in. diameter h-BN wafers with significant thicknesses had not been undertaken. In this study, we present the successful growth using HVPE of h-BN wafers with diameter of 6 in. and thickness of 40 μm with excellent crystalline quality and thickness uniformity.

The HVPE growth process was conducted in a custom-built quartz reactor using c-plane 6 in. diameter sapphire. Boron chloride (BCl_3) and ammonia (NH_3) were utilized as carbon-free precursors for B and N, respectively. To enhance the uniformity of the wafers, a rotation mechanism for the susceptor was employed at a rotation speed of 20 rpm. Initially, a 30 nm thick h-BN buffer layer was deposited at 1300 °C, followed by ramping up the temperature to 1500 °C for the growth of the active h-BN layer. The growth process was carried out under three different pressures (P = 80, 40, and 20 Torr, with 20 Torr being the system limit) to investigate the impact of growth pressure on crystallinity. Characterization of crystalline quality and optical properties was performed using x-ray diffraction (XRD), selected area electron diffraction (SAED), transmission electron microscopy (TEM), and deep ultraviolet time-resolved photoluminescence (PL) spectroscopy measurements. The PL system consists of an excitation source featuring a frequency-quadrupled femtosecond (fs) Ti: sapphire laser with 150 fs pulse width and excitation photon energy of 6.35 eV (195 nm) to provide above band-to-band excitation. The PL emission was analyzed through a 1.3 m monochromator in conjunction with a single photon counting system, equipped with a micro-channel plate photomultiplier tube (MCP-PMT) providing a 20 ps time resolution.[46]

Figure 1 shows the layer thickness profile across the entire wafer with 6 in. diameter, measured by a thickness profiler, demonstrating excellent thickness uniformity for a 40 μm thick wafer. The inset displays an optical image, exhibiting the expected transparency characteristic of a UWBG semiconductor with an energy bandgap of 6.1 eV.

Figure 2(a) plots XRD patterns in a θ–2θ scan of h-BN grown under different pressures (P). At P = 80 Torr, the (002) peak corresponding to stacked planes in the c-direction is centered at 2θ = 26°, indicating a c-lattice constant of 6.8 Å for the turbostratic phase (t-BN). This increased lattice constant in association with the t-phase BN suggests a poor layer stacking sequence along the c axis. With a decrease in pressure to P = 40 Torr, a second peak at 26.7° corresponding to the h-phase of BN emerges, signifying a transition from disordered t-phase to ordered h-phase BN. At the lowest pressure, P = 20 Torr, the peak at 26° related to the t-phase is completely absent and the only one dominant peak at 26.7° corresponds to a c-lattice constant of 6.67 Å, approaching the ideal value of phase pure h-BN. These results establish that growth at the minimum pressure of our HVPE system (P = 20 Torr) yields h-BN wafers with highest crystalline quality and thickness uniformity. Given the fixed growth temperature, the results depicted in Fig. 2 suggest that low-pressure growth effectively minimizes parasitic pre-reactions in the gas phase. As in the MOCVD growth process,[50,51] lower
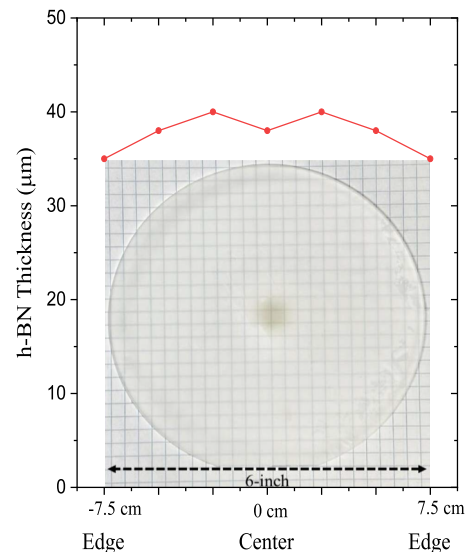

FIG. 1. Thickness profile across whole the h-BN wafer with 6 in. diameter grown at P = 20 Torr. The inset is an optical image of the wafer.

pressure growth enhances the mean free path for precursor molecules, thereby reducing the occurrence of gas-phase reactions that could generate undesired by-products or compounds.[50,51]

Figure 2(b) plots the variation of the (002) peak FWHM as a function of growth pressure. At P = 80 Torr, the XRD 2θ peak appearing at 26° has a broad FWHM of 1.41° due to the presence stacking disorder (t-BN). XRD spectrum of the sample grown at P = 40 Torr consisting of two peaks at ~26° and 26.7°, corresponding to t-BN phase and well-ordered h-BN phase, respectively, was analyzed by using two peak fitting, yielding FWHM ~0.91° for t-BN and 0.36° for h-BN. At P = 20 Torr, only a single sharp (002) peak appears at 26.7° with a FWHM = 0.35°, confirming attainment of phase-pure h-BN. The continuing narrowing of the (002) peak and the disappearance of the t-BN peak with lowering the growth pressures indicate improved structural order along the c axis. These results show that reducing growth pressure during HVPE improves the crystal structure of h-BN by limiting unwanted gas-phase reactions and promoting an improved stacking order. The observed FWHM of = 0.35° for the sample grown at 20 Torr is approaching the value of 4 inch h-BN wafers as we reported previously.[35,47]

Another notable change we made was the use of N_2 gas as a carrier gas instead of H_2 gas, as we reported previously.[35,47] Our results seem to suggest that the flow of the N_2 inert gas is more effective than H_2 in displacing and flushing out residual process gases and reaction by-products. This purging process also seems helpful in cleaning the growth environment and prevents contamination during subsequent growth steps. Overall, the combination of reduced pressure growth and the use of N_2 inert gas and carbon-free precursors appear to help minimize impurities in the gas phase and promote the deposition of epitaxial layers with improved crystalline quality and reduced defect density. Figure 3 presents secondary ion mass spectrometry (SIMS) data for two different h-BN samples. The first sample, grown using H_2 carrier gas, shows a concentration of hydrogen impurities as high as 2×10^{21} cm^{-3}, whereas the second sample,
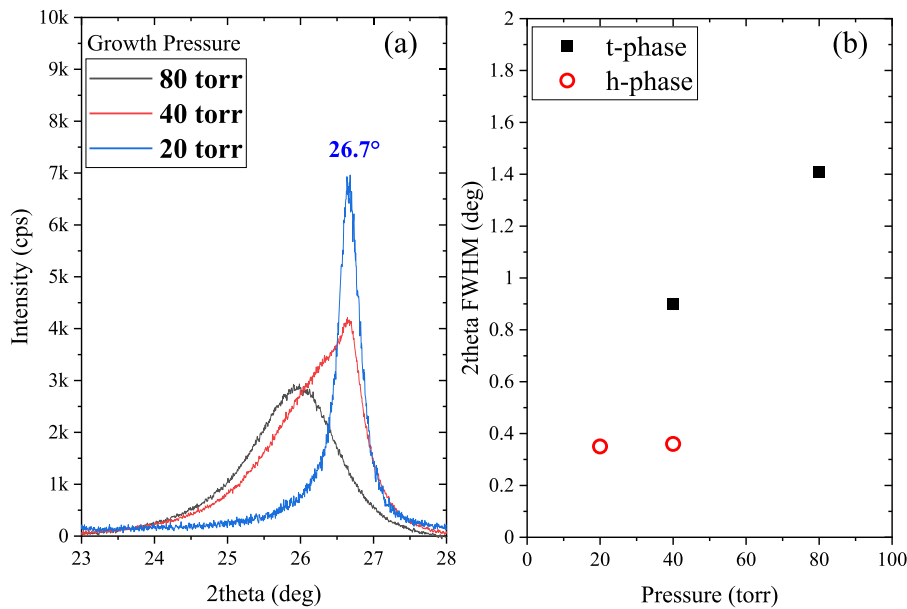
FIG. 2. (a) XRD θ–2θ scan patterns of h-BN wafer 6 in. in diameter grown by HVPE with different pressures. (b) Growth pressure vs XRD θ–2θ FWHM.

grown using N_2 as a carrier gas, exhibits a significantly lower H concentration. This confirms that eliminating hydrogen carrier gas from the reactor environment effectively reduces H impurity concentration, leading to higher-purity h-BN films. Hydrogen impurities in h-BN tend to form interstitial hydrogen (H_i) or form complexes with native defects.[52]

The selected area electron diffraction (SAED) pattern presented in Fig. 4(a) exhibits bright spots aligned along the c axis and c-plane, confirming the crystalline nature of the h-BN wafer grown at P = 20 Torr. The vertical bright spots on the SAED pattern indicate the crystalline structure along the c axis, with a layer spacing of

3.33 Å (corresponding to half of the c-lattice constant) in agreement with XRD measurements and the expected value of phase pure h-BN shown schematically in Fig. 4(b). The diffraction spots along the c-plane on the SAED pattern reflect the atomic spacing within the
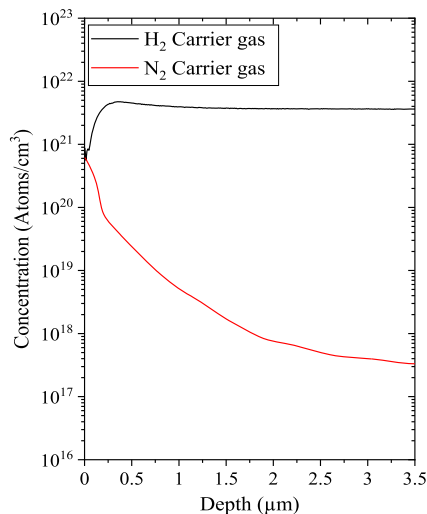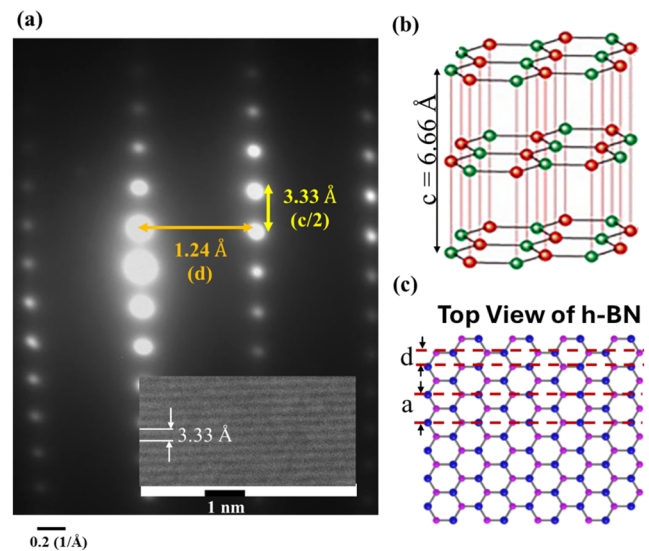

FIG. 4. (a) Selected area electron diffraction (SAED) pattern of the sample grown at P = 20 Torr. The bright spots are indicative of the crystalline structure of the h-BN sample with bright spots distance in vertical (horizontal) direction indicates c (a) lattice constant. the inset image is the cross-sectional view of the TEM image of the same sample, measuring a spacing of 3.33 Å between the stacked layers in the c-direction. (b) Schematic of the crystalline structure of h-BN, illustrating its layered structure with the c-constant of 6.66 Å (c) Schematic of top view for the crystalline structure of the h-BN wafer, where d = a/2 and a is the in-plane lattice constant.

FIG. 3. Secondary ion mass spectrometry (SIMS) analysis of hydrogen impurity concentration in two h-BN samples grown using H_2 and N_2 as a carrier gas.

c-plane, providing d = 1.24 Å (half of the *a*-lattice constant), resulting in a measured *a*-lattice constant of *a* = 2d = 2.48 Å. This value aligns well with the expected *a*-lattice constant of 2.50 Å of h-BN, as shown schematically in Fig. 4(c).

The inset image in Fig. 4(a) displays the cross-sectional transmission electron microscopy (TEM) image of the wafer grown at the lowest pressure of 20 Torr. The image clearly delineates the layered crystalline structure of h-BN, with a measured spacing between adjacent layers in the c-direction of 3.33 Å, corresponding to a c-lattice constant of 6.66 Å. This value matches perfectly with value measured by SAED as well as with the anticipated c-lattice constant of the ideal h-BN crystalline structure depicted in Fig. 4(b) and is also consistent with the XRD findings for the wafer grown at P = 20 Torr shown in Fig. 2. TEM and SAED results exhibit strong correlation with the expected values and further validate the well-defined layered crystalline structure of these BN wafers with 6 in. diameter h- produced at lowest pressure (P = 20 Torr).

Figure 5(a) presents a room temperature photoluminescence (PL) emission spectrum of the sample grown at P = 20 Torr under 195 nm excitation. In comparison with our 100 μm thick wafers with 4 in. diameter wafers, which exhibit a weaker band-edge emission line near 5.9 eV in addition to a dominant emission peak near 3.6 eV related to boron vacancy and hydrogen complex defects,[35] the PL spectrum shown in Fig. 5 reveals a dominant emission line at 3.41 eV and the band-edge emission is absent. In Fig. 5(b), the temporal response of the 3.41 eV emission line is depicted, showing a single exponential decay described by $(t) = A\,e^{-t/\tau}$, with an observed decay lifetime of τ = 2.74 ns. The measured nanosecond decay lifetime rules out the possibility of the 3.41 eV emission line being a donor–acceptor pair (DAP) transition, which typically exhibits decay lifetimes in the microsecond to millisecond range. Only impurity-to-band type transitions, apart from the band-edge transitions, are anticipated to have recombination lifetimes on the

order of nanoseconds. Upon analyzing the calculated energy levels of potential point defects in h-BN, a nitrogenvacancy (V_N)-related donor positioned at 3.48 eV above the valence band edge[52] is identified. Therefore, the dominant emission line at 3.41 eV most likely involves the transition between V_N donors and the valence band in these 6 in. diameter h-BN wafers.[53] The absence of the band-edge transition is presumably due to the presence of a high concentration of V_N impurities in the 6 in. diameter wafer studied here. Our previous investigations have explored the relationship between optical emission properties and ammonia flow rate during the MOCVD growth of h-BN thin epilayers. The earlier results have shown that sufficient nitrogen supply is essential to achieve h-BN epilayers with high optical quality.[46]

In summary, we present the first successful growth of h-BN wafers with 6 in. diameter using HVPE methods with carbon-free precursors. Our findings highlight the significance of growth pressure as a crucial parameter influencing crystalline quality, with lower growth pressure proving advantageous in reducing parasitic reactions between precursors in the gas phase. Growth carried out at the minimal pressure of 20 Torr, utilizing inert N_2 as a carrier and separation gas, resulted in more uniform growth and higher crystalline quality, as indicated by XRD, SAED, and TEM that demonstrated c-lattice and a-lattice constants approaching the ideal bulk values. Photoluminescence studies unveiled a dominant emission line at 3.41 eV, attributed to the recombination between nitrogen vacancy and the valence band. While further enhancements in the growth conditions of wafers with 6 in. diameter should focus on refining processes to enhance nitrogen supply during HVPE growth, achieving 6 in. diameter wafers with high crystalline quality marks a significant milestone. This achievement paves the way for the practical application of h-BN, transitioning it from fundamental research to the development of technologically important and cost-effective devices.
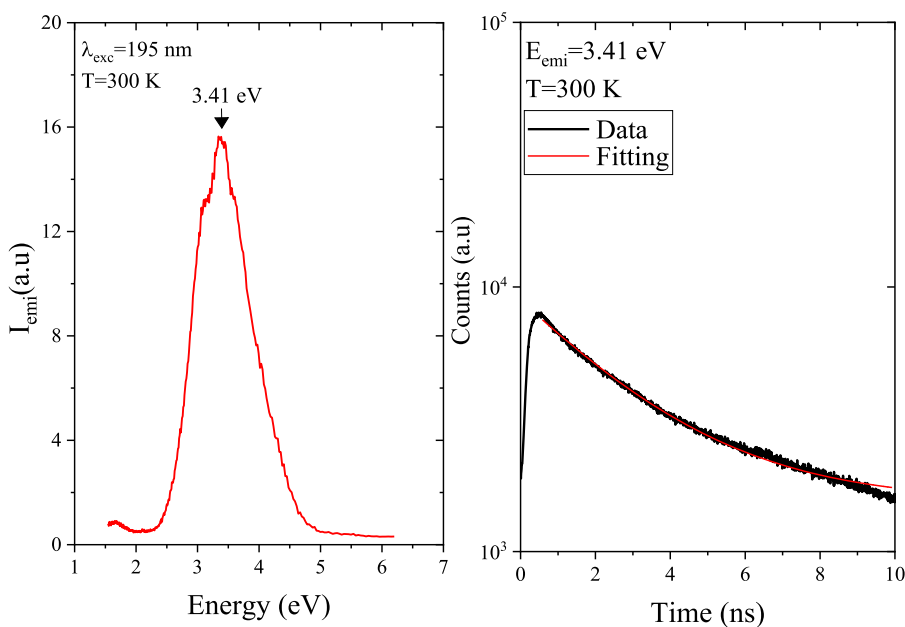
FIG. 5. (a) Room temperature (T = 300 K) photoluminescence (PL) under 195 nm laser excitation. (b) Temporal response of the 3.41 eV emission line in h-BN grown at P = 20 Torr measured at 300 K. The solid red curve is the least-squares fit of data (black dots) with a single exponential decay.

AUTHOR DECLARATIONS

Conflict of Interest

The authors have no conflicts to disclose.

Author Contributions

Z. Alemoush: Data curation (equal); Formal analysis (equal); Investigation (equal); Software (equal); Validation (equal); Visualization (equal); Writing – original draft (equal). **M. Almohammad**: Data curation (equal); Formal analysis (equal); Investigation (equal); Software (equal); Validation (equal); Visualization (equal). **J. Li**: Formal analysis (equal); Investigation (equal); Methodology (equal); Project administration (equal); Software (equal); Supervision (equal); Validation (equal); Visualization (equal). **J. Y. Lin**: Conceptualization (equal); Funding acquisition (equal); Investigation (equal); Methodology (equal); Project administration (equal); Resources (equal); Supervision (equal); Validation (equal); Visualization (equal); Writing – review & editing (equal). **H. X. Jiang**: Conceptualization (equal); Funding acquisition (equal); Investigation (equal); Methodology (equal); Project administration (equal); Resources (equal); Supervision (equal); Validation (equal); Visualization (equal); Writing – review & editing (equal).

DATA AVAILABILITY

The data that support the findings of this study are available within the article.

REFERENCES

[1] O. Slobodyan, J. Flicker, J. Dickerson, J. Shoemaker, A. Binder, T. Smith, S. Goodnick, R. Kaplar, and M. Hollis, "Analysis of the dependence of critical electric field on semiconductor bandgap," J. Mater. Res. **37**, 849 (2022).

[2] T. Sugino, K. Tanioka, S. Kawasaki, and J. Shirafuji, "Characterization and field emission of sulfur-doped boron nitride synthesized by plasma-assisted chemical vapor deposition," Jpn. J. Appl. Phys. **36**, L463 (1997).

[3] K. Watanabe, T. Taniguchi, and H. Kanda, "Direct-bandgap properties and evidence for ultraviolet lasing of hexagonal boron nitride single crystal," Nat. Mater. **3**, 404 (2004).

[4] B. Arnaud, S. Lebègue, P. Rabiller, and M. Alouani, "Huge excitonic effects in layered hexagonal boron nitride," Phys. Rev. Lett. **96**, 026402 (2006).

[5] Y. Kubota, K. Watanabe, O. Tsuda, and T. Taniguchi, "Deep ultraviolet light-emitting hexagonal boron nitride synthesized at atmospheric pressure," Science **317**, 932 (2007).

[6] G. Cassabois, P. Valvin, and B. Gil, "Hexagonal boron nitride is an indirect bandgap semiconductor," Nat. Photonics **10**, 262 (2016).

[7] Y. Hattori, T. Taniguchi, K. Watanabe, and K. Nagashio, "Anisotropic dielectric breakdown strength of single crystal hexagonal boron nitride," ACS Appl. Mater. Interfaces **8**, 27877 (2016).

[8] Y. Hattori, T. Taniguchi, K. Watanabe, and K. Nagashio, "Comparison of device structures for the dielectric breakdown measurement of hexagonal boron nitride," Appl. Phys. Lett. **109**, 253111 (2016).

[9] C. Yuan, J. Li, L. Lindsay, D. Cherns, J. W. Pomeroy, S. Liu, J. H. Edgar, and M. Kuball, "Modulating the thermal conductivity in hexagonal boron nitride via controlled boron isotope concentration," Commun. Phys. **2**, 43 (2019).

[10] H. Amano, N. Sawaki, I. Akasaki, and Y. Toyoda, "Metalorganic vapor phase epitaxial growth of a high quality GaN film using an AlN buffer layer," Appl. Phys. Lett. **48**, 353 (1986).

[11] S. Nakamura, T. Mukai, and M. Senoh, "Candela-class high-brightness InGaN/AlGaN double-heterostructure blue-light-emitting diodes," Appl. Phys. Lett. **64**, 1687 (1994).

[12] A. Khan, K. Balakrishnan, and T. Katona, "Ultraviolet light-emitting diodes based on group three nitrides," Nat. Photonics **2**, 77 (2008).

[13] Z. Zhang, M. Kushimoto, T. Sakai, N. Sugiyama, L. J. Schowalter, C. Sasaoka, and H. Amano, "A 271.8 nm deep-ultraviolet laser diode for room temperature operation," Appl. Phys. Express **12**, 124003 (2019).

[14] M. A. Khan, R. A. Skogman, R. G. Schulze, and M. Gershenzon, "Electrical properties and ion implantation of epitaxial GaN, grown by low pressure metalorganic chemical vapor deposition," Appl. Phys. Lett. **42**, 430 (1983).

[15] M. Asif Khan, A. Bhattarai, J. N. Kuznia, and D. T. Olson, "High electron mobility transistor based on a GaN-Al$_x$Ga$_{1-x}$N heterojunction," Appl. Phys. Lett. **63**, 1214 (1993).

[16] I. C. Kizilyalli, O. B. Spahn, and E. P. Carlson, "Recent progress in wide-bandgap semiconductor devices for a more electric future," ECS Trans. **109**, 3 (2022).

[17] Y. H. Chen, J. Encomendero, C. Savant, V. Protasenko, H. G. Xing, and D. Jena, "Electron mobility enhancement by electric field engineering of AlN/GaN/AlN quantum-well HEMTs on single-crystal AlN substrates," Appl. Phys. Lett. **124**, 152111 (2024).

[18] H. Amano, Y. Baines, E. Beam, M. Borga, T. Bouchet, P. R. Chalker, M. Charles *et al.*, "The 2018 GaN power electronics roadmap," J. Phys. D: Appl. Phys. **51**, 163001 (2018).

[19] P. Bagheri, C. Quiñones-Garcia, D. Khachariya, S. Rathkanthiwar, P. Reddy, R. Kirste, S. Mita, J. Tweedie, R. Collazo, and Z. Sitar, "High electron mobility in AlN:Si by point and extended defect management," J. Appl. Phys. **132**, 185703 (2022).

[20] J. Wu, W. Walukiewicz, K. M. Yu, J. W. Ager III, E. E. Haller, H. Lu, W. J. Schaff, Y. Saito, and Y. Nanishi, "Small band gap bowing in In$_{1-x}$Ga$_x$N alloys," Appl. Phys. Lett. **80**, 4741 (2002).

[21] S. Vanka, B. Zhou, R. A. Awni, Z. Song, F. A. Chowdhury, X. Liu, H. Hajibabaei, W. Shi, Y. Xiao, I. A. Navid, A. Pandey, R. Chen, G. A. Botton, T. W. Hamann, D. Wang, Y. Yan, and Z. Mi, "InGaN/Si double-junction photocathode for unassisted solar water splitting," ACS Energy Lett. **5**, 3741 (2020).

[22] S. X. Jin, J. Li, J. Z. Li, J. Y. Lin, and H. X. Jiang, "GaN microdisk light emitting diodes," Appl. Phys. Lett. **76**, 631 (2000).

[23] H. X. Jiang, S. X. Jin, J. Li, J. Shakya, and J. Y. Lin, "III-nitride blue microdisplays," Appl. Phys. Lett. **78**, 1303 (2001).

[24] J. Day, J. Li, D. Y. C. Lie, C. Bradford, J. Y. Lin, and H. X. Jiang, "III-nitride full-scale high-resolution microdisplays," Appl. Phys. Lett. **99**, 031116 (2011).

[25] H. Jiang and J. Lin, "How we made the microLED," Nat. Electron. **6**, 257 (2023).

[26] P. J. Parbrook, B. Corbett, J. Han, T. Y. Seong, and H. Amano, "Micro-light emitting diode: From chips to applications," Laser Photonics Rev. **15**, 2000133 (2021).

[27] A. K. Geim and I. V. Grigorieva, "Van der Waals heterostructures," Nature **499**, 419 (2013).

[28] R. Bourrellier, S. Meuret, A. Tararan, O. Stéphan, M. Kociak, L. H. G. Tizei, and A. Zobelli, "Bright UV single photon emission at point defects in h-BN," Nano Lett. **16**, 4317 (2016).

[29] N. R. Jungwirth, B. Calderon, Y. Ji, M. G. Spencer, M. E. Flatté, and G. D. Fuchs, "Temperature dependence of wavelength selectable zero-phonon emission from single defects in hexagonal boron nitride," Nano Lett. **16**, 6052 (2016).

[30] G. F. Knoll, *Radiation Detection and Measurement*, 4th ed. (John Wiley & Sons, 2010).

03 June 2025 19:43:07

[31] O. Osberghaus, "Die isotopenhäufigkeit des bors. massenspektrometrische untersuchung der elektronenstoßprodukte von BF3 und BCl3," Z. Phys. **128**, 366 (1950).

[32] A. Maity, S. J. Grenadier, J. Li, J. Y. Lin, and H. X. Jiang, "Hexagonal boron nitride: Epitaxial growth and device applications," Prog. Quantum Electron. **76**, 100302 (2021).

[33] T. C. Doan, S. Majety, S. Grenadier, J. Li, J. Y. Lin, and H. X. Jiang, "Fabrication and characterization of solid-state thermal neutron detectors based on hexagonal boron nitride epilayers," Nucl. Instrum. Methods Phys. Res., Sect. A **748**, 84 (2014).

[34] A. Maity, S. J. Grenadier, J. Li, J. Y. Lin, and H. X. Jiang, "High efficiency hexagonal boron nitride neutron detectors with 1 cm^2 detection areas," Appl. Phys. Lett. **116**, 142102 (2020).

[35] Z. Alemoush, A. Tingsuwatit, A. Maity, J. Li, J. Y. Lin, and H. X. Jiang, "Status of h-BN quasi-bulk crystals and high efficiency neutron detectors," J. Appl. Phys. **135**, 175704 (2024).

[36] A. Tingsuwatit, A. Maity, S. J. Grenadier, J. Li, J. Y. Lin, and H. X. Jiang, "Boron nitride neutron detector with the ability for detecting both thermal and fast neutrons," Appl. Phys. Lett. **120**, 233503 (2022).

[37] T. Ishii and T. Sato, "Growth of single crystals of hexagonal boron nitride," J. Cryst. Growth **61**, 689 (1983).

[38] N. D. Zhigadlo, "Crystal growth of hexagonal boron nitride (hBN) from Mg–B–N solvent system under high pressure," J. Cryst. Growth **402**, 308 (2014).

[39] J. Li, C. Yuan, C. Elias, J. Wang, X. Zhang, G. Ye, C. Huang *et al.*, "Hexagonal boron nitride single crystal growth from solution with a temperature gradient," Chem. Mater. **32**, 5066 (2020).

[40] Y. Li, V. Garnier, P. Steyer, C. Journet, and B. Toury, "Millimeter-scale hexagonal boron nitride single crystals for nanosheet generation," ACS Appl. Nano Mater. **3**, 1508 (2020).

[41] H. X. Jiang and J. Y. Lin, ECS J. Solid State Sci. Technol. **6**, Q3012 (2016).

[42] P. Vuong, T. Moudakir, R. Gujrati, A. Srivastava, V. Ottapilakkal, S. Gautier, P. L. Voss, S. Sundaram, J. P. Salvestrini, and A. Ougazzaden, "Scaling up of growth, fabrication, and device transfer process for GaN-based LEDs on H-BN templates to 6-inch sapphire substrates," Adv. Mater. Technol. **8**, 2300600 (2023).

[43] T. C. Doan, J. Li, J. Y. Lin, and H. X. Jiang, "Growth and device processing of hexagonal boron nitride epilayers for thermal neutron and deep ultraviolet detectors," AIP Adv. **6**, 075117 (2016).

[44] K. Ahmed, R. Dahal, A. Weltz, J.-Q. Lu, Y. Danon, and I. B. Bhat, "Growth of hexagonal boron nitride on (111) Si for deep UV photonics and thermal neutron detection," Appl. Phys. Lett. **109**, 113501 (2016).

[45] X. Yang, S. Nitta, K. Nagamatsu, S.-Y. Bae, H.-J. Lee, Y. Liu, M. Pristovsek, Y. Honda, and H. Amano, "Growth of hexagonal boron nitride on sapphire substrate by pulsed-mode metalorganic vapor phase epitaxy," J. Cryst. Growth **482**, 1 (2018).

[46] X. Z. Du, J. Li, J. Y. Lin, and H. X. Jiang, "The origins of near band-edge transitions in hexagonal boron nitride epilayers," Appl. Phys. Lett. **108**, 052106 (2016).

[47] Z. Alemoush, N. K. Hossain, A. Tingsuwatit, M. Almohammad, J. Li, J. Y. Lin, and H. X. Jiang, "Toward achieving cost-effective hexagonal BN semi-bulk crystals and BN neutron detectors via halide vapor phase epitaxy," Appl. Phys. Lett. **122**, 012105 (2023).

[48] Y. Kumagai, T. Yamane, and A. Koukitu, "Growth of thick AlN layers by hydride vapor-phase epitaxy," J. Cryst. Growth **281**, 62 (2005).

[49] Y. Kumagai, K. Goto, T. Nagashima, R. Yamamoto, M. Boćkowski, and J. Kotani, "Influence of growth rate on homoepitaxial growth of AlN at 1450 °C by hydride vapor phase epitaxy," Appl. Phys. Express **15**, 115501 (2022).

[50] G. B. Stringfellow, *Organometallic Vapor-phase Epitaxy: Theory and Practice* (Elsevier Science, 2012).

[51] F. Lévy, "Film growth and epitaxy: Methods," Encycl. Condens. Matter Phys. **2**, 210 (2005).

[52] L. Weston, D. Wickramaratne, M. Mackoit, A. Alkauskas, and C. G. Van de Walle, "Native point defects and impurities in hexagonal boron nitride," Phys. Rev. B **97**, 214104 (2018).

[53] J. Li, J. Y. Lin, and H. X. Jiang, "Fundamental optical transitions in hexagonal boron nitride epilayers," APL Mater. **12**, 111115 (2024).

03 June 2025 19:43:07